HUMAN BREAST NUMERICAL MODEL GENERATION BASED ON DEEP LEARNING FOR PHOTOACOUSTIC IMAGING

Yaxin Ma, Caiwen Jiang

Abstract

Photoacoustic imaging which combines high contrast of optical imaging and high resolution of ultrasound imaging, can provide functional information, potentially playing a crucial role in the study of breast cancer diagnostics. However, open source dataset for PA imaging research is insufficient on account of lacking clinical data. To tackle this problem, we propose a method to automatically generate breast numerical model for photoacoustic imaging. The different type of tissues is automatically extracted first by employing deep learning and other methods from mammography. And then the tissues are combined by mathematical set operation to generate a new breast image after being assigned optical and acoustic parameters. Finally, breast numerical model with proper optical and acoustic properties are generated, which are specifically suitable for PA imaging studies, and the experiment results indicate that our method is feasible with high efficiency.

1. Introduction

Photoacoustic (PA) imaging is an emerging imaging technology with non-invasive and non-ionizing advantages. PA imaging detects ultrasonic signals generated by tissue which is excited by pulsed laser [1]. During the imaging process, the tissue undergoes thermal expansion after laser irradiation, forming an initial sound field inside the tissue. The propagating sound waves, i.e. PA waves, outwards from the tissue are received by the ultrasonic transducers. After that, the initial sound field is reconstructed by the received PA signals and proper reconstruction algorithm to obtain the optical absorption distribution of the tissue [2].

PA imaging combines the optical absorption contrast and ultrasonic resolution in deep scattering tissue, which can provide functional information, such as blood oxygenation [3], beyond anatomical imaging done by traditional methods. So that it can better help cancer diagnostics, e.g. early-stage breast cancer [4-6].

However, as an emerging biomedical imaging technology, PA imaging is still in preclinical stage, and lacks clinical data, resulting in insufficient open source dataset for PA imaging research. To solve this problem, some researchers develop models comprised of simple objects [7, 8]. However, the model they proposed ignores a lot of crucial information, and unable to represent the real human breast information. Some recent studies have reported more realistic breast models [9], such as three realistic numerical breast phantoms [10], which however is manually generated suffering huge time consumption and insufficiency. In this paper, we propose to automatically generate PA numerical model datasets of human breast based on deep learning, which conforms to both anatomical and pathological features, and can reflect both optical and acoustic properties of the breast tissue. To the best of our knowledge, this is the first time applying deep learning algorithm to numerical model generation for PA imaging. The generated dataset will be available at https://github.com/YaxinMa/Numerical-Model-for-Human-Breast

2. Method

The objective of this paper is to design and implement the algorithm for automatically generating photoacoustic numerical models from mammography dataset. The steps of the algorithm are shown in below flowchart in Fig. 1. Firstly, different tissues of breast are extracted by different extraction algorithms, having done that, new images are synthesized with the extracted tissues by mathematical set operation. Finally, different tissues in new image modes are assigned with photoacoustic parameters based on their specific optical and acoustic properties.

The CBIS-DDSM (Curated Breast Imaging Subset of DDSM) dataset is an upgraded version of DDSM (Digital Database for Screening Mammography), which contains 10,239 processed mammography [11]. In order to implement the algorithm better, we preprocess the dataset by data augmentation. In particular, manual cropping was performed to process the fibroglandular tissue, which is the input of convolutional neural network based on the guidance of clinicians.

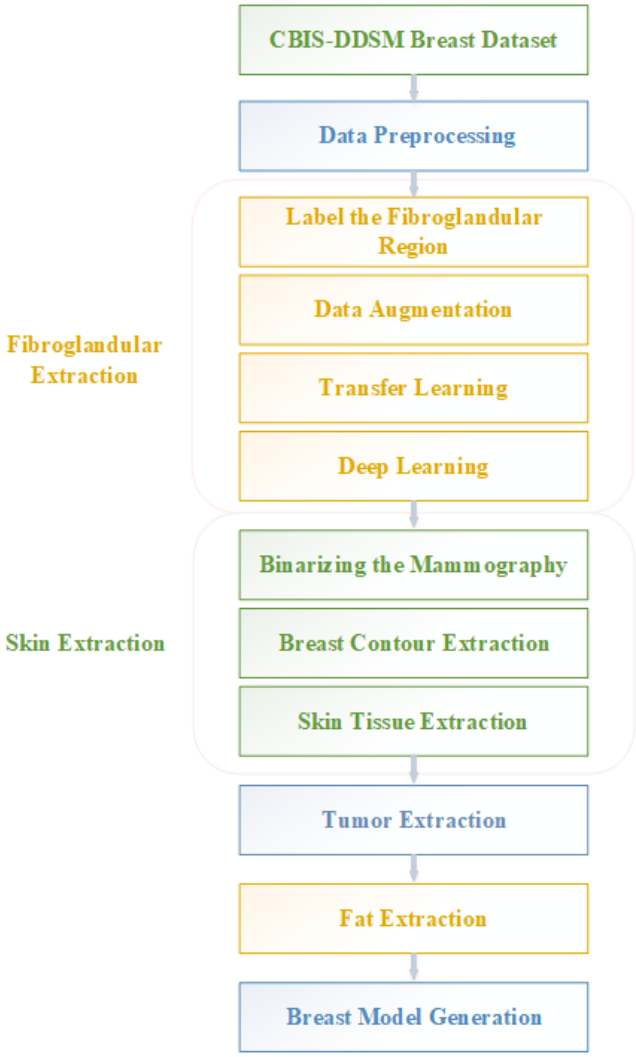

Figure 1: Flowchart of Algorithm for Automatically Generating Photoacoustic Numerical Models

The breast can be mainly divided into four types of tissues: skin, fat, fibroglandular, and tumor. Different algorithms are utilized when extracting different types of tissues. Among them, extracting fibroglandular is the most crucial and difficult task in this paper, which is the key to the implementation of automatic generation of photoacoustic numerical model dataset. The feature extraction of fibroglandular is complicated, because its shape is irregular and has no clear boundary, so that even manual labeling is very troublesome. Deep learning provides an effective automatic extraction method, which has been widely used in the field of medical image segmentation. In this paper, we use the Unet to extract fibroglandular. The architure of Unet is shown in figure 2. We also utilize classification models such as efficientNet、ResNet、VGG16、DenseNet、Inception to substitute encoder. EfficientNet is a new type of convolutional neural network based on a new model scaling method proposed by Google [12]. The performance measurement indexes include loss, Iou score and f1 score.

We use Dice loss and Focal loss function to evaluate fibroglandular segmentation performance, which is defined as:

$$L = L(precision, recall) + L(gt, pr), \quad (1)$$

The Dice loss is defined as:

$$L(precision, recall) = 1 - (1+b^2)\frac{precision \times recall}{b^2 \times precision + recall}, \quad (2)$$

Wherein, b represents the coefficient for precision and recall balance.

The Focal loss is defined as:

$$L(gt, pr) = -gta(1-pr)^g \log(pr) - (1-gt)a\,pr^g \log(1-pr), \quad (3)$$

Among them, gt represents ground truth, pr represents prediction, a is weighting factor, g represents focusing parameter.

In order to extract skin, edge extraction algorithm is used to get the outline of the breast, having done that, the skin tissue can be obtained by further processing the outline. The tumor is provided by the CBIS-DDSM data set readily and can be extracted easily. After extracting the above three tissues, the fat tissue can be assigned to the rest of the breast.

After extracting all the four types of breast tissues, PA breast numerical models are then automatically synthesized by these tissues. In PA breast models, each pixel is labeled with a specific type of breast tissue: skin, fat, fibroglandular or tumor. After that, each pixel is assigned with specific optical and acoustic parameters (e.g. optical absorption / scattering coefficients, acoustic velocity, density, etc.) for PA imaging research. Finally, realistic 2-D breast numerical phantom for PA imaging is completed.

3. Experiments

3.1. Dataset Processing

For ease of processing, the dataset is firstly converted from a Dicom medical image format to BMP format image, and then resized to 320×600 pixels. In order to obtain a better segmentation performance, the input image is subjected to data enhancement operations, such as smoothing, histogram equalization, and binarization.

In particular, for fibroglandular extraction, we manually label the fibroglandular region on the CBIS-DDSM breast

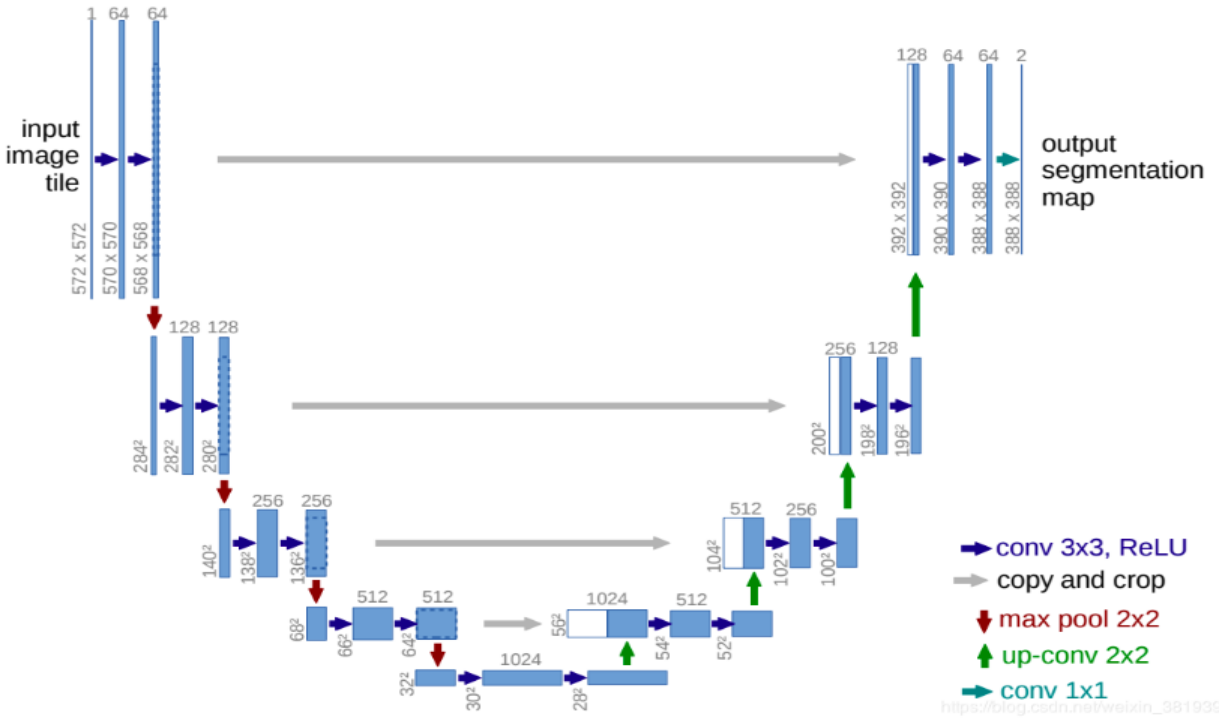

Figure 2: The architecture of Unet

image as the input training sample of the deep learning model. The output of the deep learning model is the result of automatically segmented fibroglandular region. In order to expand the volume of training examples, data augmentation is applied including horizontal flipping, vertical flipping, rotation, contrast adjustment, which is shown in Fig. 3. Finally, a total number of 1,400 extracted fibroglandular datasets were produced, which were divided into three parts: training set, verification set and test set according to the ratio of 6:2:2.

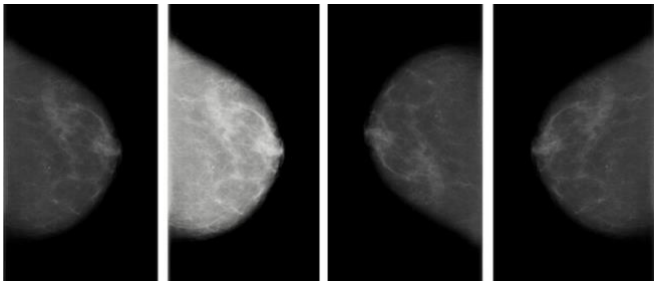

(a) (b) (c) (d)

Figure 3: The operation of data augmentation. They are (a) original image, (b) contrast adjustment, (c) rotation, (d) horizontal flipping.

3.2. Extraction of different type of tissues

The skin tissue is obtained by extracting the outline of breast shown in Fig. 4. Firstly, the mammography is binarized shown in Fig. 4(b). And then the edge extraction algorithm using the canny operator is applied to segment the outline of breast shown in Fig. 4(c). Finally, we utilize morphological processing such as expansion and corrosion to generate skin model (shown in Fig. 4(d)) in accordance with real breast skin data.

Deep learning is applied to extract fibroglandular tissues of breast. Unet is exploited with 1,400 preprocessed datasets. Transfer learning that transfers the pre-trained parameters on the ImageNet dataset is also employed to tackle the problem of small samples. Adam optimizer is used to optimize the model, and Sigmoid function is utilized as classification function. The learning rate is set to 0.0001, epoch is 100, and the batch size is 8. This experiment was implemented on a server with four NVIDIA GTX1080Ti installed.

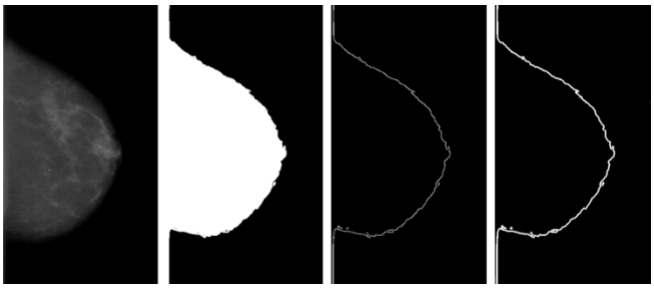

(a) (b) (c) (d)

Figure 4: The operation of skin extraction. They are (a)original image, (b)binarization, (c)edge extraction algorithm, (d)morphological processing such as expansion and corrosion

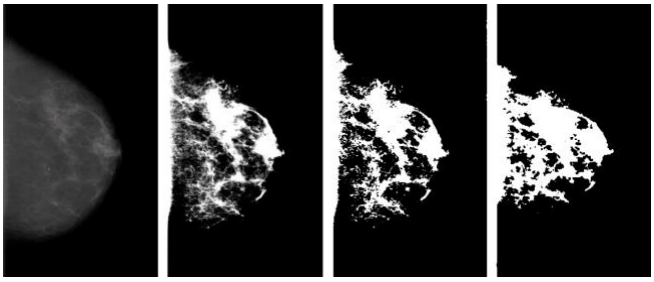

(a) (b) (c) (d)

Figure 5: The comparison between ground truth and output of deep learning model for breast firboglandular tissue segmentation. They are (a)the original image, (b)ground truth, (c)ground truth after binarization, (d)output of deep learning model.

The segmentation result of the model is shown in Figure 5, and the performance measurement including loss, Iou score, f1 score are shown in Table 1. It can be clearly seen that the segmented images based on the deep learning model is quite similar to ground truth.

Table 1: Performance Measurement of Segmentation Results(EfficientNet)

	Training set	Verification set
Loss	0.3334	0.3071
Iou_score	0.7539	0.7943
F1-score	0.8583	0.8807

Note: TP = true positive, FP = false positive, TN = true negative, FN = false negative. Iou score = TP/(TP+FP+FN), F1 score = (2P·R)/(P+R), P = TP/(TP+FP), R = TP/(TP+FN)

Table 2. Performance Measurement of different network

Model	Loss	Iou_score	F1-score
VGG16	0.36569	0.76083	0.86149
Resnet50	0.30757	0.79495	0.88355
Densenet121	0.30046	0.80163	0.88802
inceptionV3	0.33961	0.33961	0.87534

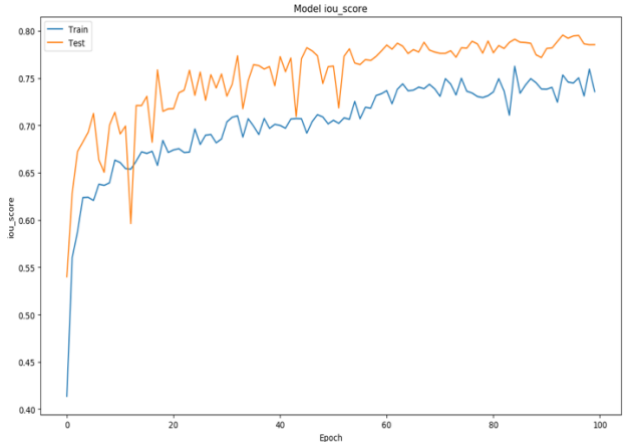

Figure 6: The performance of iou score of Densenet121

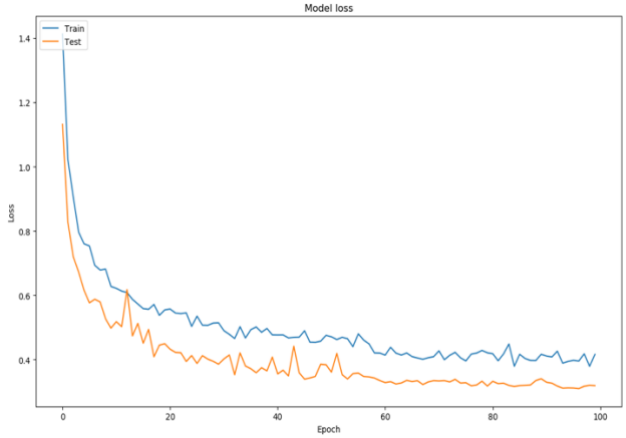

Figure 7: The performance of loss of Densenet121

A union operation is executed on the extracted skin, fibroglandular, and tumor tissues, then the fat tissue is obtained by subtracting the union from the original mammography.

After dividing the various tissues of the breast, these tissues are employed to synthesize new breast numerical models. From bottom to top, is the new model includes four

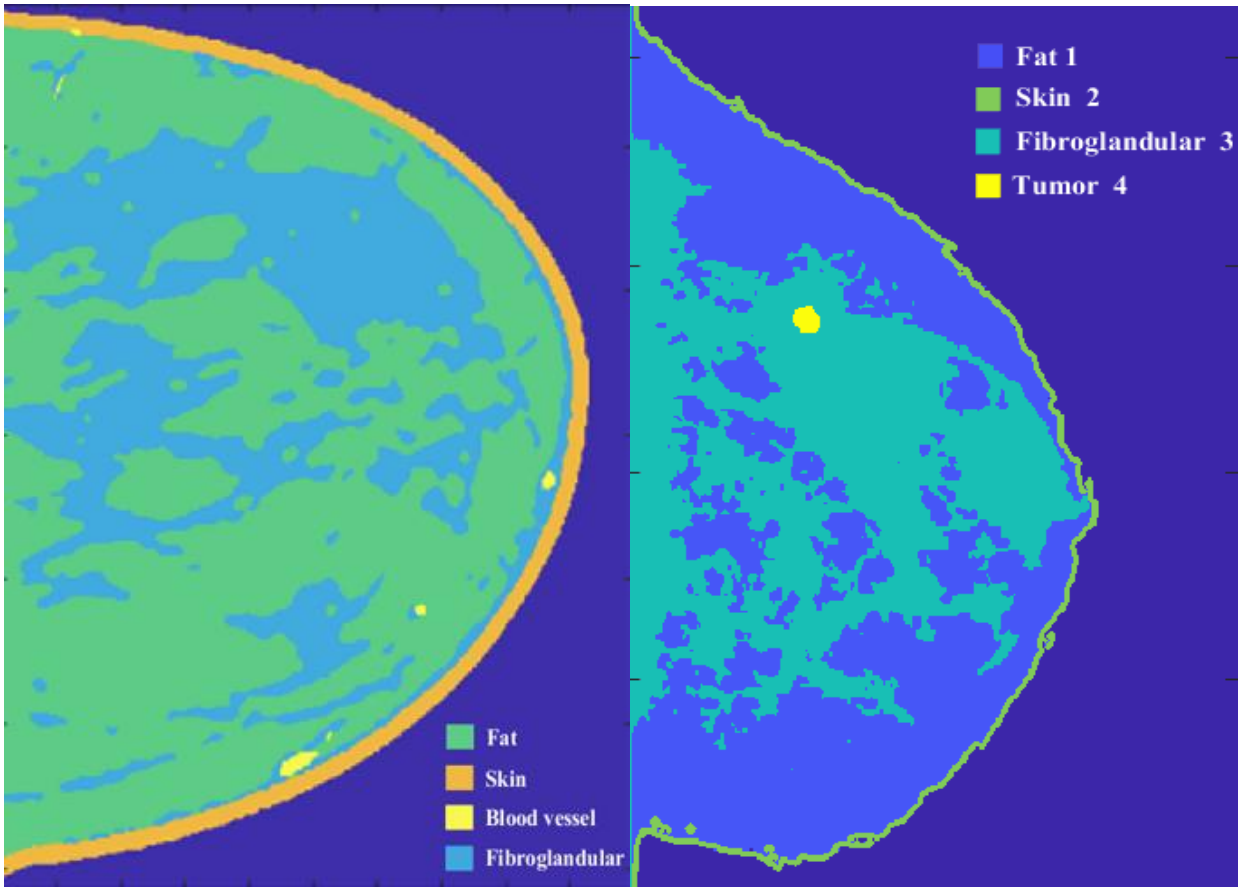

(a) (b)

Figure 8: The comparison between (a) manual generation result and (b) automatic generation result from our method.

layers: fat, skin, fibroglandular, and tumor. Index are exploited to represent different tissues in the synthesized numerical models. The Index corresponding to fat, skin, fibroglandular, and tumors are represented as 1, 2, 3, and 4.

The manually segmented breast slice result in [10] and the automatically generated breast numerical image models in this paper are shown in Fig. 8 for comparison. It can be seen that the automatically generated image is very similar to the manually extracted breast slice image, proving the feasibility and accuracy of our proposed algorithm.

Finally, because different tissues have their specific optical and acoustic parameters [13, 14], the synthesized numerical image model is further assigned with different values shown in Table 3. After doing that, the automatic generation of breast numerical image data is completed for photoacoustic imaging.

Table 3: Optical and Acoustic Parameters of Tissues

Tissue type	Index	$\mu_a(cm^{-1})$	$\mu_s(cm^{-1})$	$v(m/s)$
Fat	1	0.05	159	1470
Skin	2	0.08	500	1650
Fibroglandular	3	0.04	133	1515
Tumor	4	0.07	16	1548

Note: μ_a indicates optical absorption coefficient, μ_s indicates optical scattering coefficient, v indicates sound speed.

4. Conclusion

In this paper, we automatically generated batches of breast numerical model images with proper optical and acoustic characteristics, which can be used for PA imaging research. The crucial step is to extract fibroglandular tissue, which is achieved by deep learning and transfer learning. The results show that deep learning method demonstrates good performance in breast fibroglandular tissue

segmentation, thereby eliminating manual cropping used in previous literatures, and significantly improving efficiency.

In short, in order to solve the problem of insufficient photoacoustic image dataset, we propose a method to automatically generate photoacoustic image dataset by extracting, synthesizing and assigning parameters to clinically obtained breast tissues from mammography. Our future research will focus on improving segmentation algorithm performance, adding breast vascular tissue in the breast images, and automatically generating 3D PA numerical image data.

References

[1] Y. Zhou, J. Yao, and L. V. Wang, "Tutorial on photoacoustic tomography," J Biomed Opt, vol. 21, no. 6, p. 61007, Jun 2016.

[2] L. V. Wang, "Tutorial on Photoacoustic Microscopy and Computed Tomography," IEEE Journal of Selected Topics in Quantum Electronics, vol. 14, no. 1, pp. 171-179, 2008.

[3] C. Yang, H. Lan, H. Zhong, and F. Gao, "Quantitative photoacoustic blood oxygenation imaging using deep residual and recurrent neural network," in 2019 IEEE 16th International Symposium on Biomedical Imaging (ISBI 2019), 2019, pp. 741-744: IEEE.

[4] L. V. Wang and J. Yao, "A practical guide to photoacoustic tomography in the life sciences," Nat Methods, vol. 13, no. 8, pp. 627-38, Jul 28 2016.

[5] C. Yang and F. Gao, "EDA-Net: Dense Aggregation of Deep and Shallow Information Achieves Quantitative Photoacoustic Blood Oxygenation Imaging Deep in Human Breast," in Medical Image Computing and Computer Assisted Intervention – MICCAI 2019(Lecture Notes in Computer Science, 2019, pp. 246-254.

[6] H. Lan et al., "Ki-GAN: Knowledge Infusion Generative Adversarial Network for Photoacoustic Image Reconstruction In Vivo," in Medical Image Computing and Computer Assisted Intervention – MICCAI 2019(Lecture Notes in Computer Science, 2019, pp. 273-281.

[7] C. Huang, K. Wang, L. Nie, L. V. Wang, and M. A. J. a. p. a. Anastasio, "Full-Wave Iterative Image Reconstruction in Photoacoustic Tomography with Acoustically Inhomogeneous Media," 2013.

[8] K. Wang, S. A. Ermilov, R. Su, H. P. Brecht, A. A. Oraevsky, and M. A. Anastasio, "An imaging model incorporating ultrasonic transducer properties for three-dimensional optoacoustic tomography," IEEE Trans Med Imaging, vol. 30, no. 2, pp. 203-14, Feb 2011.

[9] B. Deng, D. H. Brooks, D. A. Boas, M. Lundqvist, and Q. Fang, "Characterization of structural-prior guided optical tomography using realistic breast models derived from dual-energy x-ray mammography," Biomed Opt Express, vol. 6, no. 7, pp. 2366-79, Jul 1 2015.

[10] Y. Lou, W. Zhou, T. P. Matthews, C. M. Appleton, and M. A. Anastasio, "Generation of anatomically realistic numerical phantoms for photoacoustic and ultrasonic breast imaging," J Biomed Opt, vol. 22, no. 4, p. 41015, Apr 1 2017.

[11] R. S. Lee, F. Gimenez, A. Hoogi, K. K. Miyake, M. Gorovoy, and D. L. Rubin, "A curated mammography data set for use in computer-aided detection and diagnosis research," Sci Data, vol. 4, p. 170177, Dec 19 2017.

[12] M. Tan and Q. V. J. a. p. a. Le, "EfficientNet: Rethinking Model Scaling for Convolutional Neural Networks," 2019.

[13] S. Sarkar, A. A. Gurjarpadhye, C. G. Rylander, and M. Nichole Rylander, "Optical properties of breast tumor phantoms containing carbon nanotubes and nanohorns," J Biomed Opt, vol. 16, no. 5, p. 051304, May 2011.

[14] N. Honda, K. Ishii, T. Terada, T. Nanjo, and K. Awazu, "Determination of the tumor tissue optical properties during and after photodynamic therapy using inverse Monte Carlo method and double integrating sphere between 350 and 1000 nm," J Biomed Opt, vol. 16, no. 5, p. 058003, May 2011.